Molecular Pharmacology Fast Forward. Published on December 21, 2010 as doi:10.1124/mol.110.067611

MOL Manuscript # 67611

Molecular Dissection of Dual Pseudosymmetric Solute Translocation Pathways in Human P-Glycoprotein

Zahida Parveen, Thomas Stockner, Caterina Bentele, Sandra Pferschy, Martin Kraupp, Michael Freissmuth, Gerhard F. Ecker and Peter Chiba*

Institute of Medical Chemistry, Medical University of Vienna, Waehringerstrasse 10, A-1090 Vienna, Austria, (ZP, TS, CB, SP, MK, PC)

Institute of Pharmacology, Medical University of Vienna, Waehringerstrasse 13A, 1090 Vienna, Austria, (MF)

Emerging Field Pharmacoinformatics, Dept. of Me dicinal Chemistry, University of Vienna, Althanstrasse 14, A-1090 Vienna, Austria (GFE)

Molecular Pharmacology Fast Forward. Published on December 21, 2010 as DOI: 10.1124/mol.110.067611
This article has not been copyedited and formatted. The final version may differ from this version.

Running title page

a) Dual P-gp solute translocation pathways

b) Address correspondence to: Peter Chiba, Institute of Medical Chemistry, Waehringerstrasse 10, A-1090 Vienna, Austria, phone: +43 1 4277 60806, Fax: +43 1 4277 9608, E-mail: peter.chiba@meduniwien.ac.at

c)

Number of text pages: 20

Number of tables 2

Number of figures 6

Number of references 39

Number of words in:

Abstract 250 words

Introduction 749 words

Discussion 1551 words

d) List of non-standard abbreviations

ABC, ATP-binding cassette; P-gp, P-glycoprotein; MDR, multidrug resistance; TMD, transmembrane domain; NBD, nucleotide binding domain;

Molecular Pharmacology Fast Forward. Published on December 21, 2010 as DOI: 10.1124/mol.110.067611
This article has not been copyedited and formatted. The final version may differ from this version.

Abstract

The human multispecific drug efflux transporter P-glycoprotein causes drug resistance and modulates the pharmacological profile of systemically administered medicines. It has arisen from a homodimeric ancestor by gene duplication. Crystal-structures of mouse MDR1A indicate that P-gp shares the overall architecture with two homodimeric bacterial exporters, Sav1866 and MsbA, which have complete rotational symmetry. For ABC-transporters nucleotide binding occurs in two symmetric positions in the motor domains. Based on the homology with entirely symmetric half-transporters the present study addressed the key question: Can biochemical evidence for the existence of dual drug translocation pathways in the transmembrane domains of P-gp be found? P-gp was photolabeled with propafenone analogs, purified, digested proteolytically and peptide fragments were identified by high-resolution mass-spectrometry. Labeling was assigned to two regions in the protein by projecting data into homology models. Subsequently, symmetric residue pairs in the putative translocation pathways were identified and replaced by site directed mutagenesis. Transport assays corroborated the existence of two pseudosymmetric translocation pathways. While rhodamine123 has a preference to take one path, verapamil, propafenones and vinblastine preferentially use the other. Two major findings ensued from this study: the existence of two solute translocation pathways in P-gp as a reflection of evolutionary origin from a homodimeric ancestor and selective but not exclusive use of one of these pathways by different P-gp solutes. The pseudosymmetric behavior reconciles earlier kinetic and thermodynamic data, suggesting an alternative concept of drug transport by P-gp that will aid in understanding the off-target quantitative structure activity relationships of P-gp interacting drugs.

Molecular Pharmacology Fast Forward. Published on December 21, 2010 as DOI: 10.1124/mol.110.067611
This article has not been copyedited and formatted. The final version may differ from this version.

Introduction

P-glycoprotein (P-gp, ABCB1) is a primary active multispecific drug efflux transporter, which is considered a major determinant of the pharmacokinetic, safety and efficacy profile of drugs. Recent recommendations of the International Transporter Consortium (Giacomini et al., 2010) have incorporated a decision tree for determination of P-gp solute properties during early drug development. P-glycoprotein is an ATP-binding cassette (ABC) transporter, which uses the energy of nucleotide-binding and hydrolysis to prevent xenotoxic compounds from entering the cell. It is composed of two transmembrane domains which are responsible for translocation of solutes and two nucleotide binding domains, which provide the energy for outward transport of solutes. Recently published crystal structures of mouse MDR1A (Aller et al., 2009) indicate that P-gp shares the twisted topology of Sav1866, a homodimeric bacterial multidrug transporter (Dawson and Locher, 2006; Dawson and Locher, 2007). A common architecture is also observed with the corrected structures of the bacterial lipid A transporter MsbA (Ward et al., 2007).

While our understanding of ATP-binding and hydrolysis has improved through the availability of a number of structurally resolved ABC-importers and isolated nucleotide binding domains (NBDs) of ABC-exporters (see Seeger and van Veen, 2009 for review), the mechanism of solute binding and transport remains elusive. Two crystal structures of mouse P-gp co-crystallized in the presence of the cyclic hexapeptide inhibitors QZ59-SSS and QZ59-RRR (PDB ID: 3G60, 3G61) show these ligands to be located at the interface of the two transmembrane domains (TMDs) in either a central position (QZ59-RRR) (between helices 6 and 12) or in two asymmetric positions (QZ59-SSS) termed “upper” and “lower” site, corroborating the notion that binding of solutes takes place at the interface of the two transmembrane domains (Aller et al., 2009). The wide open inward facing inverted V-conformation of this structure, in which the NBDs are at a distance of 20Å is binding competent, but might not

Molecular Pharmacology Fast Forward. Published on December 21, 2010 as DOI: 10.1124/mol.110.067611
This article has not been copyedited and formatted. The final version may differ from this version.

correspond to a physiological state, because P-gp cross-linked between residues 175 and 820 in the cytoplasmic portion of transmembrane helices 3 and 9 is able to hydrolyze ATP in the absence of solutes. Also, basal ATPase activity is stimulated by solutes, indicating that under conditions in which the NBDs cannot disassociate completely, the transporter is still able to bind drugs (Loo et al., 2010).

It is generally believed that the central pore represents an expansive binding pocket for solutes, which accommodates ligands by interaction with a large complement of amino acid residues (Loo et al., 2009; Loo and Clarke, 2008). During exit solutes take a translocation path, which requires at least the following steps: 1) Entry of the solute into the translocation pathway from the inner leaflet, 2) a conformational rearrangement of the transporter (the rate limiting step, which provides access of the solute to the alternate side of the membrane) and 3) exit of the solute into the cell exterior. This process is powered by binding and hydrolysis of ATP.

Photolabeling with propafenone analogs in the nucleotide free state was previously used to probe the binding sites of P-gp (Pleban et al., 2005). Photolabeling of the benzophenone biradical species proceeds via reaction with any closely located C-H bonds in the protein. In the present study these data were projected into models of human P-gp in the nucleotide bound and free state, based on crystal structures of Sav1866 (Dawson and Locher, 2006) and mouse P-gp (Aller et al., 2009). Photolabeling is expected to capture the step of carrier reorientation, which may be considered the most highly populated conformational state of the protein. In all models the C-alpha distance between the most intensely labeled residues in TM helices 5 and 11 was found to be 23 to 32Å. Given the size of both, the amino acid side chains and the photoactive carbonyl-group in the ligand, this distance between the two photolabeled regions is best explained by the existence of two pseudosymmetric rather than one single solute translocation pathway for propafenones.

Molecular Pharmacology Fast Forward. Published on December 21, 2010 as DOI: 10.1124/mol.110.067611
This article has not been copyedited and formatted. The final version may differ from this version.

In further support of this model we generated transporter mutants, in which access of positively charged compounds to one of the two photolabeled regions was prevented by introducing single arginine residues in each of the putative translocation paths in pseudosymmetric positions of the protein. Our results are compatible with a model where the preferred translocation path for rhodamine123 takes it into vicinity of residue Q773 in helix 8, while verapamil, vinblastine and propafenone analogs preferentially take a path that brings them close to residue Q132 in helix 2. In the wild-type transporter residues Q773 and Q132 do not interact with solutes, but arginine substitutions cause diagnostic changes in transport or inhibitory potencies of positively charged compounds. Interaction of uncharged compounds with P-gp was not affected by arginine substitutions. This confirmed that mutation of Q-residues at positions 132 and 773 did not disrupt the molecular mechanics of the transporter.

Molecular Pharmacology Fast Forward. Published on December 21, 2010 as DOI: 10.1124/mol.110.067611
This article has not been copyedited and formatted. The final version may differ from this version.

Materials and Methods

Sequence Alignments and Homology Modeling. Multiple sequence alignments of ABCB proteins were performed using ClustalW. The models of human P-gp were based on the crystal structures of Sav1866 (PDB ID: 2HYD; 3.0 Å resolution) and of mouse P-gp (PDB ID: 3G5U; 3.8Å resolution) (Aller et al., 2009) using MODELLER (version 9v2) (Marti-Renom et al., 2000; Sali and Blundell, 1993) in the automodel protocol with the refinement set to "very_slow". 20 models were generated with each of the templates. The data-driven models based on Sav1866 (Dawson and Locher, 2006) (PDB ID: 2HYD) have been described previously (Stockner et al., 2009) (PMDB ID: PM0075213). Model quality was assessed using the DOPE (Shen and Sali, 2006) and GA341 scores (Melo and Sali, 2007) of MODELLER, ProQ (Wallner and Elofsson, 2003) and ProCheck (Laskowski et al., 1993) . The models with the lowest MODELLER objective function were selected for visualization. Propafenone labeling data (Pleban et al., 2005) were mapped onto the human P-gp structure by adding labeling intensity on a per residue basis.

Construction of P-gp Mutants. Site directed mutagenesis was performed at positions 132 and 773 of hexa-his tagged human P-gp cloned into the entry vector pENTR4-MDR1-His_6 to generate the Q132A, Q132R, Q773A, Q773R and the Q132A/Q773A mutants using the following forward and reverse primers: Q132A-f 5'- CTG CTT ACA TTG CGG TTT CAT TTT GG-3', Q132A-r 5'- CCA AAA TGA AAC CGC AAT GTA AGC AG-3', Q132R-f 5'- GCT GCT TAC ATT CGT GTT TCA TTT TG-3', Q132R-r 5'- CAA AAT GAA ACA CGA ATG TAA GCA GC-3', Q773A-f 5'- CAT TTT TCC TTG CGG GTT TCA CAT TTG GC-3', Q773A-r 5'- GCC AAA TGT GAA ACC CGC AAG GAA AAA TG-3', Q773R-f 5'- CAT TTT TCC TTC GAG GTT TCA CAT TTG-3', Q773R-r 5'- CAT TTT TCC TTC GAG GTT TCA CAT TTG-3'. Double mutant Q132R/Q773R was generated by restriction digestion of pENTR4-Q132R and pENTR4-Q773R with *Sal*1 and *EcoR*1 and subsequent

Molecular Pharmacology Fast Forward. Published on December 21, 2010 as DOI: 10.1124/mol.110.067611
This article has not been copyedited and formatted. The final version may differ from this version.

ligation of the mutated fragment from pENTR4-Q773R into pENTR4-Q132R using T4 DNA ligase (rapid DNA ligation kit, Fermentas, Vienna, Austria). The wild type and mutant P-gp were then transferred to the pCEP4 destination vector using gateway cloning (Hartley et al., 2000).

Expression of P-gp Mutants. Wild type or mutant P-gp was transiently expressed in HEK-293/EBNA cells (obtained from the University of Bielefeld, Germany). Cells were trypsinized, harvested and centrifuged at 500g when being sub-confluent. The cell pellet was incubated on ice water with the mouse monoclonal - P-gp specific - MRK16 antibody (5µg/mL) (Kamiya Biomedical Company, Seattle, WA, USA) and IgG2A (2.5µg/mL) as the control antibody for 30 min. Cells were then washed with ice cold PBS and centrifuged at 500g followed by a 30min incubation on ice water with an FITC labeled goat anti mouse secondary antibody (12.5µg/mL). After incubation cells were again washed with ice cold PBS and centrifuged. Cells were then resuspended in DMEM medium and measured in a FACSCalibur flow cytometer (Becton Dickinson, Vienna, Austria).

Rhodamine123 Efflux Assays. Transiently transfected HEK-293/EBNA cells were trypsinized, centrifuged at 500g and the cell pellets were resuspended in DMEM medium containing rhodamine123 (Sigma Chemical Co., St. Louis, MO) at a final concentration of 0.2µg/ml (0.53µmol/l). Cell suspensions were incubated at 37°C for 30min. The selection of 37°C for preloading of cells was selected, because the compound is not taken up to any significant extent on ice water. Tubes were chilled on ice and cells were harvested at 500g in an Eppendorf 5403 centrifuge (Eppendorf, Hamburg, Germany). The cell pellet was washed with ice cold DMEM medium (pH 7.4) and centrifuged at 500g. Supernatants were removed, and the cell pellet was resuspended in DMEM medium (pH 7.4) pre-warmed to 37°C. After 60, 120, 180, 240 and 300 seconds aliquots of the incubation mixture were transferred to tubes containing an equal volume of ice-cold stop solution (DMEM medium containing GPV31 at a final concentration of 5µmol/l). Aliquots drawn at the

Molecular Pharmacology Fast Forward. Published on December 21, 2010 as DOI: 10.1124/mol.110.067611
This article has not been copyedited and formatted. The final version may differ from this version.

respective time points were kept in an ice water bath and measured within 1h on a Becton Dickinson FACSCalibur flow cytometer (Becton Dickinson, Vienna, Austria). Viable cells were selected by setting appropriate gates for forward and side scatter. The excitation and emission wavelengths were 488nm and 534nm, respectively.

Inhibition Assays. IC_{50} values for rhodamine123 efflux inhibition were determined as reported (Chiba et al., 1996). Briefly, cells were sedimented, the supernatant was removed by aspiration, and the cells were resuspended at a density of 1 x 10^6/ml in DMEM medium containing rhodamine123 (Sigma Chemical Co., St. Louis, MO) at a final concentration of 0.2µg/ml (0.53µmol/l). Cell suspensions were incubated at 37°C for 30 min. Tubes were chilled on ice and centrifuged at 500g in an Eppendorf 5403 centrifuge (Eppendorf, Hamburg, Germany). Supernatants were removed, and the cell pellet was resuspended in medium pre-warmed to 37°C containing either no inhibitor or compounds at various concentrations ranging from 8nM to 50µM, depending on the solubility and expected potency of the inhibitor. Eight concentrations (serial 1:2.5 dilution) were tested for each inhibitor. After 60, 120, 180 and 240 seconds, aliquots of the incubation mixture were transferred to tubes containing an equal volume of ice-cold stop solution (DMEM medium containing GPV31 at a final concentration of 5µmol/l). Zero time points were determined by immediately pipetting rhodamine123-preloaded cells into ice cold stop solution. Samples drawn at the respective time points were kept in an ice water bath and measured within 1h on a Becton Dickinson FACSCalibur flow cytometer (Becton Dickinson, Vienna, Austria). Viable cells were selected by setting appropriate gates for forward and side scatter. The excitation and emission wavelengths were 488nm and 534nm, respectively. Five thousand gated events were accumulated for the determination of mean fluorescence values. Exponentials were fitted to the data points taken at different times allowing estimation of the flux rate for the zero time point. The experimental protocol would not require normalization for protein expression, because IC_{50}

Molecular Pharmacology Fast Forward. Published on December 21, 2010 as DOI: 10.1124/mol.110.067611
This article has not been copyedited and formatted. The final version may differ from this version.

values, in contrast to first order rate constants, are independent of protein expression. First order rate constants were then used to generate concentration response curves, from which the IC_{50} values were calculated as 50% occupancy values.

Data Analysis. Concentration-response curves for inhibitors (verapamil, GPV31, GPV366) were fitted to a four parameter logistic equation (i.e., the Hill equation with a term for background diffusion) using a Marquardt-Levenberg algorithm. In those instances, where the slope factor (Hill coefficient) differed from 1, the data points were also subjected to non- linear-least-squares curve fitting to e quations describing the inhibition via one and two sites. A s tatistically significant improvement by the t wo-site model was verified by an F-test based on the extra sum of squares principle. Averages of IC_{50} values were compared using one way ANOVA applying Duncan's multiple range test in SPSS (10.0). A *P* value of 0.05 was considered as significant. Data are represented as mean ± S.E.

Results

Photolabeling of P-gp with Propafenone Analogs. Previously obtained photolabeling data (Pleban et al., 2005) were projected into models of human P-glycoprotein, based on the template structures of Sav1866 in the nucleotide bound state (Fig. 1A) and a previously published data-driven model of P-gp based on the same template, in which the diverging helical bundles in the transmembrane domains were rotated towards each other (Stockner et al., 2009) (PMDB ID: PM0075213; Fig. 1B). A third model was based on the recently published mouse MDR1A crystal structure in the nucleotide free state (Fig. 1C) (Aller et al., 2009). Quality parameters for these models are given in Table 1. The quality of all models was high according to the parameters described in the legend for Table 1. C-alpha atoms of the most intensely photolabeled residues A311 and L312 (right magenta spheres in

Molecular Pharmacology Fast Forward. Published on December 21, 2010 as DOI: 10.1124/mol.110.067611
This article has not been copyedited and formatted. The final version may differ from this version.

Figs 1A-C) and F951, S952 and Y953 (left magenta spheres in Figs. 1A-C) are shown in van der Waals rendering. In all three models the distances between these residues exceeded the size of the affinity ligands, suggesting that these amino acid residues were unable to r eact with one single propafenone molecule simultaneously. Models thus indicate that binding of propafenone analogs occurs in two separate pseudosymmetric regions at the interface of the TMDs, involving helix 5 and adjacent helix 8, as well as helix 11. The C-alpha distance between photolabeled residues is 32Å in the nucleotide bound state (Fig. 1A), 24Å in the data-driven model (Fig. 1B) and 23Å in the model based on mouse MDR1A (Fig. 1C). For comparison a propafenone (GPV51) (Pleban et al., 2005) sized to same scale as the models is shown in a balls and sticks representation in Fig. 1D.

The irradiation-induced bi-radical species of the carbonyl group in the benzophenone moiety shows a preference for methionine residues (Dorman and Prestwich, 1994). Helices 5 and 8 as well as their immediate vicinity are devoid of methionine residues and thus a reaction preference due to the presence of methionines can be ruled out. In contrast, helix 11, which lies in a pseudosymmetric position with respect to helix 5, contains two methionine residues, which are accessible to the ligands. The presence of these methionine residues in TM11 might explain that the adjacent helix 2, in contrast to helix 8 in the N-terminus, is not strongly labeled. The area in between the two photolabeled regions, mainly made up of helices 6 and 12, does not show labeling, indicating that the photoactive group is not oriented towards these helices. Additional labeling was observed for residue M197 and its vicinity in TM3. This helix is not part of either of the two photolabeled regions discussed above. M197 however is predicted by the homology model to be membrane exposed and close to one of the portals of P-gp in the nucleotide free crystal structure (Aller et al., 2009). Labeling of this residue is thus indicative of an – albeit conjectural - path along which solutes might access the central cavity of the transporter from the inner leaflet of the membrane.

Molecular Pharmacology Fast Forward. Published on December 21, 2010 as DOI: 10.1124/mol.110.067611
This article has not been copyedited and formatted. The final version may differ from this version.

Analysis of Photolabeling Data and Design of Mutants. Would data discussed in the previous section be indicative of the existence of two pseudosymmetric transport pathways and could these paths be dissected biochemically? Many of the more than 1000 known P-gp solutes are protonable compounds. We therefore engineered P-gp arginine mutants in which the positive charge of the amino acid residue was expected to block the transport of positively charged solutes, when positioned in or close to the respective transport path. Uncharged compounds served as controls for an unaltered functionality of the transporter.

Selection of candidate residues for site directed mutagenesis was based on the following criteria: i) pore exposure ii) conservation in symmetric positions, iii) predicted location within the inner leaflet and iv) a position that lies within the putative transport path and proximal of the photolabeled regions. Two polar glutamine residue pairs, Q132 (TM2)/Q773 (TM8) and Q195 (TM3)/Q838 (TM9) were compliant with those criteria. The first of these two pairs was selected, because residues are closer to the photolabeled regions in helices 5/8 and 11 and conserved in all annotated P-gp sequences, but not in all ABCB family members. *D. discoideum* ABCB subfamily full transporters (gi18496816, gi18496818) contain an arginine residue in a position aligning with Q773 of human ABCB1. In addition the *D. discoideum* half transporters ABCB5 and 6 (Q819W2, Q54RU1) contain an arginine residue in a position aligning with residue Q132 of the human ABCB1 sequence and *Xenopus tropicalis* subfamily B member 4 (gi39645391) contains an arginine residue in a position aligning with Q773 in human P-gp. Therefore an arginine residue was expected to be tolerated in positions 132 and 773. Figure 2 shows stereo images of the Sav1866 based P-gp model, in which a transversal cross section along the central axis of the pore allows a view from the pore, centered on the helix 2/11 interface in Fig. 2A and the helix 5/8 interface in Fig. 2B. Figures are rotated 180° with respect to each

other. The mutated residues Q132 and Q773 are shown to be pore exposed and depicted in green and orange color, respectively. C-alpha atoms of most intensely photolabeled residues are shown as magenta spheres. The ClustalW conservation score and relative orientation of residues in TM helices 2 and 8 are shown in Fig. 2C. The only completely conserved and aligning residues in annotated P-gp sequences are Q132 and Q773. Also they constitute the only polar residue pair in helices 2 and 8, for which side chains are predicted to be pore exposed. Importantly, these residues are located inside the pore and not membrane exposed. Therefore, they are not located at putative gates of the protein. Figure 2D shows a top view of a Sav1866 based model of P-gp with residues in identical color as in Figs. 2A and B.

Rhodamine123 Efflux in Q132R/A and Q773R/A Mutants. In an initial series of experiments we monitored rhodamine123 efflux in HEK-293/EBNA cells transiently transfected with either wild-type P-gp or the Q132R and Q773R mutants. The previously described zero trans efflux protocol was used (Chiba et al., 1996) for the determination of first order rate constants (FORCs). A representative single experiment for rhodamine123 efflux in the Q773R mutant is shown in Fig. 3A. An exponential curve was fitted to data points taken at 1, 2, 3, 4 and 5 minutes. Details are given in the legend to Fig. 3A. FORCs depend on protein expression rates, which differ between individual experiments and also between wt and mutants. Therefore FORCs, determined as described in the legend to Fig. 3A were plotted as a function of expression in Fig. 3B. Data points for cells transfected with wild-type P-gp are shown as black triangles. The slope of the linear regression line (black stippled line) reflects the transport rate for these cells. Introduction of an arginine residue at position 132 (green triangles) decreased transport rates to 52±13% of wild type (green stippled line), while replacement of Q773 by arginine (orange data points, orange stippled line) reduced transport rates to 24±6%. A comparable

Molecular Pharmacology Fast Forward. Published on December 21, 2010 as DOI: 10.1124/mol.110.067611
This article has not been copyedited and formatted. The final version may differ from this version.

decrease in transport activity was also observed at a rhodamine123 concentration of 5μM, indicating the reaction conditions to be first order (data not shown). A mutation of both glutamine residues to arginine resulted in complete loss of transport activity (Fig. 3B, cyan data points, cyan stippled line), even though the protein was expressed at the cell surface. The residual rate is similar for all data points irrespective of expression rate (0.7-0.8/sec) and reflects outward diffusion of rhodamine123 from cells. As a control mock transfected cells were used (blue data points). These show a low flux rate corresponding to diffusion. Replacement of glutamine residues in either position 132 (yellow triangles) or 773 (magenta triangles) by alanine residues did not affect rhodamine123 transport, thereby ruling out a direct interaction of these glutamine residues with the solutes (Fig. 3B).

Effect of Propafenone Analogs on Rhodamine123 Efflux in Q132R/A and Q773R/A Mutants. Propafenone analogs are solutes and inhibitors of P-gp. These were evaluated based on experimentally determined IC_{50} values for the inhibition of rhodamine123 transport, because a direct measurement of P-gp mediated propafenone flux rates is not possible due to rapid membrane permeation by diffusion (Schmid et al., 1999). Most propafenone analogs contain a tertiary nitrogen atom, which becomes positively charged upon protonation. One of these compounds, GPV31, a p-fluorophenylpiperazine analog of propafenone (Chiba et al., 1996) was used first. For each concentration of GPV31 a time dependent decrease in mean cellular fluorescence was monitored over four minutes. A representative experiment for the Q773R mutant is shown in Fig. 4A. Details are described in the figure legend. FORCs for controls and different GPV31 concentrations were then plotted as a function of the inhibitor concentration. A representative concentration response curve determined in duplicate is shown in Fig 4B. A composite graph of the results of six independent experiments performed in duplicate is shown in Fig. 4C. For each data point the mean ± SE is given. Data are represented as

Molecular Pharmacology Fast Forward. Published on December 21, 2010 as DOI: 10.1124/mol.110.067611
This article has not been copyedited and formatted. The final version may differ from this version.

fractional inhibition values to enable comparison of values from different experiments. The IC_{50} value for wild-type P-gp was found to be 0.11±0.06µmol/l (black), while mutant Q132R showed an almost seven fold higher IC_{50} value of 0.71±0.46µmol/l (green). In contrast, the Q773R mutant showed an IC_{50} value of 0.02±0.01µmol/l (orange). A 35-fold difference in IC_{50} values was thus observed between the two mutants. In order to show that charge repulsion was indeed the underlying principle for the observed effects, the acid amide analog of propafenone, GPV366 (Ecker et al., 1999), which is not protonable and thus permanently uncharged, was used in subsequent control experiments. Again six independent experiments were performed in duplicate. IC_{50} values for wild type (black) and mutants Q132R (green) and Q773R (orange) (Fig. 5, Table 2) were indistinguishable, demonstrating that uncharged P-gp solutes were not affected by introduction of a positive charge in either position 132 or 773.

Additional experiments were performed with chalcone analogues, which are potent inhibtors of P-gp. These are uncharged compounds. Similar to GPV366 these compounds showed undistinguishable IC_{50} values in wild type and mutants (data not shown).

Effect of Verapamil and Vinblastine on Rhodamine123 Efflux in Q132R/A and Q773R/A Mutants. In a third series of experiments we evaluated the effect of verapamil and vinblastine on rhodamine123 transport in wild type and mutants Q132R and Q773R. Similar to propafenones, verapamil is a solute and inhibitor of P-gp that has been shown to bind to the Hoechst (H) -site of the protein (Al-Shawi and Omote, 2005; Al-Shawi et al., 2003; Shapiro and Ling, 1997; Spoelstra et al., 1994). First order rate constants of rhodamine123 efflux were determined at different verapamil concentration. A composite graph of 5 independent experiments performed in duplicate is shown in Fig. 6. Verapamil inhibited rhodamine123 transport of wild type P-gp with an IC_{50} value of

Molecular Pharmacology Fast Forward. Published on December 21, 2010 as DOI: 10.1124/mol.110.067611
This article has not been copyedited and formatted. The final version may differ from this version.

0.43±0.10μmol/l. In contrast, the IC_{50} values for the Q132R and Q773R mutants were 1.24±0.13 and 0.14±0.04μmol/l, respectively.

For vinblastine a composite graph of three independent experiments performed in duplicate is presented in Fig. 7. The respective IC_{50} values were 2.68±0.93μM for wild type, 0.45±0.16μM for mutant Q773R and 9.19±1.2μM for the Q132R mutant. Mutation of glutamine residues to alanine did not change IC_{50} values for GPV31, GPV366, verapamil or vinblastine (in line with the results observed for rhodamine123 efflux), suggesting that molecular mechanics and function are not altered by the mutations. Table 2 gives a synopsis of IC_{50} values for the inhibition of rhodamine123 efflux in wild type and mutants.

Biphasic Characteristics of Concentration Response Curves for GPV31 and Verapamil in Wild Type P-gp. The concentration response curves for wild type should be a composite of the concentration response curves obtained for the two mutants. In theory, two sites ought to be resolved in the wild type transporter with affinity differences of the magnitude observed above. Assuming the presence of two translocation pathways, the two sites ought to be present at a 1:1 ratio; under these conditions, an affinity difference of 10-fold ought to suffice to discriminate between one and two site models, provided that the error is sufficiently small (De Lean et al., 1982). However, these theoretical insights are based on Monte Carlo simulations, which do not necessarily recapitulate the nature of the variability in the current experiments. In addition the fact that rhodamine123 prefers one of the two sites also affects the ability to accurately discriminate between one and two site models (Nanoff et al., 1987). In fact convergence was achieved in most instances, when the data for inhibition of wild type P-gp by GPV31 and by verapamil were fitted to a two-site model. In addition, in several instances the fit to the biphasic curve resulted in a significant improvement over a monophasic inhibition curve, but

Molecular Pharmacology Fast Forward. Published on December 21, 2010 as DOI: 10.1124/mol.110.067611
This article has not been copyedited and formatted. The final version may differ from this version.

this was not uniformly seen in all experiments. We therefore conclude that the current data are consistent with the presence of two pathways for verapamil and GPV31 in wild type P-gp but that the experimental error is too large to unequivocally resolve these in concentration response curves for wild-type P-gp.

Discussion

Despite the availability of several ABC-exporter structures the molecular details of P-gp dependent solute transport remain unresolved. The availability of the mouse MDR1A structure in the nucleotide free state in complex with the cyclic hexapeptide inhibitors QZ59-SSS and QZ59-RRR (PDB ID: 3G5U, 3G60, 3G61) (Aller et al., 2009) corroborated the notion that ligands are bound at the interface of the transmembrane domains as suggested by earlier experimental evidence (Loo and Clarke, 1999; Pleban et al., 2005). The translocation pathway taken by the solutes however remained undefined.

P-gp is thought to have arisen from a half-transporter by gene duplication (Gottesman and Pastan, 1993) and has retained an overlapping solute specificity with several bacterial efflux half-transporters (Reuter et al., 2003; Velamakanni et al., 2008). These half-transporters require homodimerization for function and show complete axial rotational symmetry, implying that every structural element in the protein is found twice. Therefore solutes would choose to bind to either of two sites formed by an identical complement of amino acid residues and identical 3D structure. Ensuing ligand poses would therefore be required to represent mirror images of each other. Indeed an example of a two site cooperative behavior was found for vinblastine-binding of the bacterial half-transporter LmrA (van Veen et al., 2000). In contrast to these half transporters, P-gp is a full transporter, in which gene duplication has led to a fusion of both monomers into a single polypeptide chain. Figure 1 shows photolabeling of P-gp in two distinct pseudosymmetric regions, providing evidence that ligands are

Molecular Pharmacology Fast Forward. Published on December 21, 2010 as DOI: 10.1124/mol.110.067611
This article has not been copyedited and formatted. The final version may differ from this version.

still recognized by two -initially identical- regions of the protein. Evolutionary diversification changed properties of the se two regions in a way that make them biochemically dissectible. Results from photolabeling experiments indicate positioning of the photoactive benzophenone group in either of the two regions at the time of photo-activation and -labeling. Importantly, photolabeling is unable to discriminate between binding of solutes in either position in different P-gp molecules or simultaneous binding of t wo substrates to th e same P-gp molecule. Also, parts of a lternatively bound solute molecules might extend into and interact within an overlapping and more central region of the transporter.

In this study mutant P-gp was generated to address the question if solutes reach the two photolabeled regions via two translocation pathways that reflect the twofold rotational (pseudo)symmetry of the transmembrane domains. Positively charged arginine residues were placed in symmetric positions of the transporter to prevent positively charged ligands from reaching either of the photolabeled regions. Both the Q132R and the Q773R mutant showed reduced transport activity for rhodamine123, which however was more pronounced in the Q773R mutant. In contrast, verapamil, vinblastine and propafenone analogs were more strongly affected by mutation of residue 132 to arginine. IC_{50} values for rhodamine123 efflux inhibition in the two R-mutants differed by a factor of 8.9 for verapamil, 20 for vinblastine and 36 for the protonable propafenone analogue GPV31. Indistinguishable IC_{50} values were found for either compound in the Q132A, the Q773A and the Q132A/Q773A mutant. Also the uncharged propafenone analogue GPV366 showed identical IC_{50} values for wild type and mutants. This was also the case for an uncharged chalcone derivative. Three conclusions can be drawn from these experiments. *Firstly,* charge repulsion is the underlying principle for selectively blocking one of the solute translocation pathways. *Secondly,* glutamine residues are not directly interacting with solutes. *Thirdly,* molecular mechanics of the transporter are not altered by the mutations. Finally, these

Molecular Pharmacology Fast Forward. Published on December 21, 2010 as DOI: 10.1124/mol.110.067611
This article has not been copyedited and formatted. The final version may differ from this version.

data demonstrate that a biochemical dissection of solute translocation pathways of P-gp is possible by site directed mutagenesis and that these pathways are both used by rhodamine123, propafenone analogs, verapamil and vinblastine. While rhodamine123 shows preference for one of them, propafenones, verapamil and vinblastine are preferentially using the other.

How do these results compare to data from the literature? As early as 1997 Shapiro and Ling reported positively cooperative sites for drug transport by P-glycoprotein with distinct drug specificities. These sites were then named R- and H-site because of their preferential binding of rhodamine123 and Hoechst33342, respectively. Verapamil was reported to preferentially interact with the H-site (Shapiro and Ling, 1997). Earlier work by Spoelstra indicated daunorubicin, an R-site compound, to be inhibited by verapamil in a non-competitive fashion at low daunorubicin concentration and in a competitive manner at higher concentrations. This was interpreted as indicating that daunorubicin bound to two sites with different affinities and that verapamil bound to the lower affinity site (Spoelstra et al., 1994). In addition, Guiral et al. reported that daunorubicin was transported by P-gp in a positively cooperative manner (Guiral et al., 1994). Our findings are in accordance with a two site model and for the first time, to our knowledge, relate these sites to (pseudo)symmetric positions in the transporter. Data also do not contradict the model of multiple binding sites (Martin et al., 2000), because mutations introduced in this study block access of compounds to pseudosymmetric interaction regions, which might have partially overlapping binding properties for different chemical entities. Also, evidence for the existence of allosteric (non-substrate) solute-binding sites has been presented (Martin et al., 2000).

Evolutionary pressure seems to have led to conservation of amino acid ensembles in the TMDs of P-gp (Chiba et al., 2006). This might enable binding pockets to procure redundant binding interactions with solutes. A review on the nature of polyspecificity has appeared recently (Gutmann et al., 2010).

Highest conservation is observed for residues that are pore-exposed and these are candidate residues for interaction with solutes. While aromatic residues have been found to provide about half of the residues interacting with cyclic hexapeptide inhibitors (Aller et al., 2009), only 2 of 16 residues that interact with verapamil are aromatic (Loo and Clarke, 2008). Therefore in addition to aromatic residues, aliphatic and other polar residues do contribute to solute interaction. Interaction redundancy, as well as the ability of the transporter to accommodate more than one solute molecule at a time, do however not imply that the process of drug interaction is proceeding in a random fashion and does not contradict a twofold (pseudo)symmetric interaction of solutes with the transporter as found in this study.

In two recent reports (Loo et al., 2008; Loo et al., 2009) arginine scanning was employed for identification of residues in the solute translocation pathway of P-gp. For this purpose all residues in membrane spanning portions of the TMDs were mutated to arginine in a trafficking deficient background and rescue was used as the readout. A subset of mutants in which arginines were pore oriented, were able to enhance trafficking. The 132R mutant did not increase trafficking of the G251V background, while mutant 773R showed a complete trafficking deficiency. Therefore Loo et al. did not study these mutations further (Loo et al., 2009).

In Fig. 2D the Sav1866 based P-gp model, which is considered to represent the outward facing (low affinity, solute releasing) conformation of the transporter, either of the two mutated residues Q132 (green) and Q773 (orange) is located in one of the wing-like extensions of the structure. One wing, shown on the left, contains residue 132 and is formed by helices 1 and 2 of the N-terminal and 9, 10, 11 and 12 of the C-terminal TMD. The most intensely photolabelled residues 951 to 953 in helix 11 are shown as magenta spheres. Additional labeling is observed for adjacent C-terminal residues in TM11 (magenta ribbon). Out of 16 residues that have been identified to be important for verapamil

Molecular Pharmacology Fast Forward. Published on December 21, 2010 as DOI: 10.1124/mol.110.067611
This article has not been copyedited and formatted. The final version may differ from this version.

binding (Loo and Clarke, 2008) 11 lie in the left wing. C-alpha atoms of these residues are depicted as yellow spheres and lie at a distance of 7 to 1 5 Å from the photolabelled residues 951 to 953 in TM helix 11.

The wing shown on the right (Fig. 2D) is composed of helices 7 and 8 of the C-terminal and 3, 4, 5, and 6 of the N-terminal half of P-gp. Most strongly photolabelled residues 311 and 312 in helix 5 are again shown as magenta spheres with adjacent regions of high labeling in helices 5 and 8 shown as magenta ribbons. Five residues located in this wing have been identified to be involved in verapamil binding. These are located at a C-alpha distance of 8 to13 Å from photolabeled residues. Residues 132 and 773 adopt a position in a region of the protein, which is in contact with the inner leaflet of the membrane and closer to the cell interior than any other of the highlighted residues (magenta and yellow). This can be appreciated from the side views in Figs. 2A and B. Our data suggest that a positive charge in either of these positions selectively prevents positively charged solutes from reaching the respective interaction region within the same wing. Also, the majority of verapamil residues (11 out of 16) are located in close proximity of residue 132, which is in agreement with our findings that this part of the protein contains the preferred interaction region for verapamil.

In conclusion, two major findings ensued from this study: proof of the exis tence of two solute translocation pathways in P-gp as a reflection of evolutionary origin from a homodimeric ancestor and selective but not exclusive use of one of these pathways by different P-gp solutes. Geometric considerations suggest that these paths might partially overlap. This has important implications for the process of drug development and a molecular understanding of the interaction of P-gp with drugs.

Molecular Pharmacology Fast Forward. Published on December 21, 2010 as DOI: 10.1124/mol.110.067611
This article has not been copyedited and formatted. The final version may differ from this version.

Authorship Contribution Section

Participated in research design: Chiba, Parveen, Stockner

Conducted experiments: Parveen, Stockner, Bentele, Pferschy

Contributed new reagents or analytic tools: Stockner

Performed data analysis: Parveen, Chiba, Bentele, Freissmuth, Ecker

Wrote or contributed to the writing of the manuscript: Chiba, Parveen, Stockner, Freissmuth

Other: Chiba acquired funding for the research.

References

Al-Shawi MK and Omote H (2005) The remarkable transport mechanism of P-glycoprotein: a multidrug transporter. *J Bioenerg Biomembr* **37**(6):489-496.

Al-Shawi MK, Polar MK, Omote H and Figler RA (2003) Transition state analysis of the coupling of drug transport to ATP hydrolysis by P-glycoprotein. *J Biol Chem* **278**(52):52629-52640.

Aller SG, Yu J, Ward A, Weng Y, Chittaboina S, Zhuo R, Harrell PM, Trinh YT, Zhang Q, Urbatsch IL and Chang G (2009) Structure of P-glycoprotein reveals a molecular basis for poly-specific drug binding. *Science* **323**(5922):1718-1722.

Chiba P, Ecker G, Schmid D, Drach J, Tell B, Goldenberg S and Gekeler V (1996) Structural requirements for activity of propafenone-type modulators in P-glycoprotein-mediated multidrug resistance. *Mol Pharmacol* **49**(6):1122-1130.

Chiba P, Mihalek I, Ecker GF, Kopp S and Lichtarge O (2006) Role of transmembrane domain/transmembrane domain interfaces of P-glycoprotein (ABCB1) in solute transport. Convergent information from photoaffinity labeling, site directed mutagenesis and in silico importance prediction. *Curr Med Chem* **13**(7):793-805.

Dawson RJ and Locher KP (2006) Structure of a bacterial multidrug ABC transporter. *Nature* **443**(7108):180-185.

Dawson RJ and Locher KP (2007) Structure of the multidrug ABC transporter Sav1866 from Staphylococcus aureus in complex with AMP-PNP. *FEBS Lett* **581**(5):935-938.

De Lean A, Hancock AA and Lefkowitz RJ (1982) Validation and statistical analysis of a computer modeling method for quantitative analysis of radioligand binding data for mixtures of pharmacological receptor subtypes. *Mol Pharmacol* **21**(1):5-16.

Dorman G and Prestwich GD (1994) Benzophenone photophores in biochemistry. *Biochemistry* **33**(19):5661-5673.

Ecker G, Huber M, Schmid D and Chiba P (1999) The importance of a nitrogen atom in modulators of multidrug resistance. *Mol Pharmacol* **56**(4):791-796.

Giacomini KM, Huang SM, Tweedie DJ, Benet LZ, Brouwer KL, Chu X, Dahlin A, Evers R, Fischer V, Hillgren KM, Hoffmaster KA, Ishikawa T, Keppler D, Kim RB, Lee CA, Niemi M, Polli JW, Sugiyama Y, Swaan PW, Ware JA, Wright SH, Yee SW, Zamek-Gliszczynski MJ and Zhang L (2010) Membrane transporters in drug development. *Nat Rev Drug Discov* **9**(3):215-236.

Gottesman MM and Pastan I (1993) Biochemistry of multidrug resistance mediated by the multidrug transporter. *Annu Rev Biochem* **62**:385-427.

Guiral M, Viratelle O, Westerhoff HV and Lankelma J (1994) Cooperative P-glycoprotein mediated daunorubicin transport into DNA-loaded plasma membrane vesicles. *FEBS Lett* **346**(2-3):141-145.

Gutmann DA, Ward A, Urbatsch IL, Chang G and van Veen HW (2010) Understanding polyspecificity of multidrug ABC transporters: closing in on the gaps in ABCB1. *Trends Biochem Sci* **35**(1):36-42.

Hartley JL, Temple GF and Brasch MA (2000) DNA cloning using in vitro site-specific recombination. *Genome Res* **10**(11):1788-1795.

Laskowski RA, MacArthur MW, Moss DS and Thornton JM (1993) PROCHECK: a program to check the stereochemical quality of protein structures. *J Appl Cryst* **26**:283-291.

Loo TW, Bartlett MC and Clarke DM (2008) Arginines in the first transmembrane segment promote maturation of a P-glycoprotein processing mutant by hydrogen bond interactions with tyrosines in transmembrane segment 11. *J Biol Chem* **283**(36):24860-24870.

Loo TW, Bartlett MC and Clarke DM (2009) Identification of residues in the drug translocation pathway of the human multidrug resistance P-glycoprotein by arginine mutagenesis. *J Biol Chem* **284**(36):24074-24087.

Loo TW, Bartlett MC and Clarke DM (2010) Human P-glycoprotein is active when the two halves are clamped together in the closed conformation. *Biochem Biophys Res Commun*.

Loo TW and Clarke DM (1999) The transmembrane domains of the human multidrug resistance P-glycoprotein are sufficient to mediate drug binding and trafficking to the cell surface. *J Biol Chem* **274**(35):24759-24765.

Loo TW and Clarke DM (2008) Mutational analysis of ABC proteins. *Arch Biochem Biophys*.

Marti-Renom MA, Stuart AC, Fiser A, Sanchez R, Melo F and Sali A (2000) Comparative protein structure modeling of genes and genomes. *Annu Rev Biophys Biomol Struct* **29**:291-325.

Martin C, Berridge G, Higgins CF, Mistry P, Charlton P and Callaghan R (2000) Communication between multiple drug binding sites on P-glycoprotein. *Mol Pharmacol* **58**(3):624-632.

Melo F and Sali A (2007) Fold assessment for comparative protein structure modeling. *Protein Sci* **16**(11):2412-2426.

Nanoff C, Freissmuth M and Schutz W (1987) The role of a low beta 1-adrenoceptor selectivity of [3H]CGP-12177 for resolving subtype-selectivity of competitive ligands. *Naunyn Schmiedebergs Arch Pharmacol* **336**(5):519-525.

Pleban K, Kopp S, Csaszar E, Peer M, Hrebicek T, Rizzi A, Ecker GF and Chiba P (2005) P-glycoprotein substrate binding domains are located at the transmembrane domain/transmembrane domain interfaces: a combined photoaffinity labeling-protein homology modeling approach. *Mol Pharmacol* **67**(2):365-374.

Reuter G, Janvilisri T, Venter H, Shahi S, Balakrishnan L and van Veen HW (2003) The ATP binding cassette multidrug transporter LmrA and lipid transporter MsbA have overlapping substrate specificities. *J Biol Chem* **278**(37):35193-35198.

Sali A and Blundell TL (1993) Comparative protein modelling by satisfaction of spatial restraints. *J Mol Biol* **234**(3):779-815.

Schmid D, Ecker G, Kopp S, Hitzler M and Chiba P (1999) Structure-activity relationship studies of propafenone analogs based on P-glycoprotein ATPase activity measurements. *Biochem Pharmacol* **58**(9):1447-1456.

Seeger MA and van Veen HW (2009) Molecular basis of multidrug transport by ABC transporters. *Biochim Biophys Acta* **1794**(5):725-737.

Shapiro AB and Ling V (1997) Positively cooperative sites for drug transport by P-glycoprotein with distinct drug specificities. *Eur J Biochem* **250**(1):130-137.

Shen DW, Akiyama S, Schoenlein P, Pastan I and Gottesman MM (1995) Characterisation of high-level cisplatin-resistant cell lines established from a human hepatoma cell line and human KB adenocarcinoma cells: cross-resistance and protein changes. *Br J Cancer* **71**(4):676-683.

Shen MY and Sali A (2006) Statistical potential for assessment and prediction of protein structures. *Protein Sci* **15**(11):2507-2524.

Spoelstra EC, Westerhoff HV, Pinedo HM, Dekker H and Lankelma J (1994) The multidrug-resistance-reverser verapamil interferes with cellular P-glycoprotein-mediated pumping of daunorubicin as a non-competing substrate. *Eur J Biochem* **221**(1):363-373.

Stockner T, de Vries SJ, Bonvin AM, Ecker GF and Chiba P (2009) Data-driven homology modelling of P-glycoprotein in the ATP-bound state indicates flexibility of the transmembrane domains. *Febs J* **276**(4):964-972.

van Veen HW, Margolles A, Muller M, Higgins CF and Konings WN (2000) The homodimeric ATP-binding cassette transporter LmrA mediates multidrug transport by an alternating two-site (two-cylinder engine) mechanism. *Embo J* **19**(11):2503-2514.

Velamakanni S, Yao Y, Gutmann DA and van Veen HW (2008) Multidrug transport by the ABC transporter Sav1866 from Staphylococcus aureus. *Biochemistry* **47**(35):9300-9308.

Wallner B and Elofsson A (2003) Can correct protein models be identified? *Protein Sci* **12**(5):1073-1086.

Ward A, Reyes CL, Yu J, Roth CB and Chang G (2007) Flexibility in the ABC transporter MsbA: Alternating access with a twist. *Proc Natl Acad Sci U S A* **104**(48):19005-19010.

Molecular Pharmacology Fast Forward. Published on December 21, 2010 as DOI: 10.1124/mol.110.067611
This article has not been copyedited and formatted. The final version may differ from this version.

Footnotes

This study was supported by the Austrian Science Fund [grant # SFB3509]. Zahida Parveen is recipient of a scholarship from the Higher Education Commission Pakistan.

Address reprint requests to Peter Chiba, Institute of Medical Chemistry, Waehringerstrasse 10, A-1090 Vienna, Austria, E-mail: peter.chiba@meduniwien.ac.at

Molecular Pharmacology Fast Forward. Published on December 21, 2010 as DOI: 10.1124/mol.110.067611
This article has not been copyedited and formatted. The final version may differ from this version.

Legends for Figures.

Figure 1. Projection of photolabeling data into homology models. Top view of P-gp homology models based on the Sav1866 template structure (A), a data-driven P-gp model (B) and mouse MDR1A (C). Photolabeled residues are depicted in magenta. The N-terminal half of the protein is depicted in blue, the C-terminal half in cyan. C-alpha atoms of most intensely labeled residues are depicted as magenta spheres. Mutated residues 132 and 773 are depicted in green and orange VDW rendering, respectively. (D) Photoactive propafenone analog GP51 in ball and stick representation sized to same scale as the models.

Figure 2. Stereo images of transversal cross sections of P-gp along the central axis of the pore. Images have to be viewed in parallel eye view **A**: view on the helix 2/11 interface; residue Q132: green; photolabeled residues in magenta (refer to Fig. 1). Yellow spheres represent C-alpha atoms of residues identified to be involved in verapamil binding (Loo and Clarke, 2008). **B**: Side view on the helix 5/8 interface. Residue Q773 is depicted in an orange VDW rendering. Photolabeled residues are again shown in magenta. Yellow spheres indicate C-alpha atoms of residues involved in verapamil binding. The N-terminal half of the protein is depicted in blue, the C-terminal half is in cyan. A and B provide views, which are at an angle of 180° with respect to each other. **C**: Sequence alignment of helices 2 and 8 with conservation score in multiple sequence alignments of all annotated P-gp sequences as well as exposure to lipid, pore or towards other helices. **D**: Top view of a Sav1866 based homology model of P-gp. Residues are colored as in Figs. 2A and B.

Figure 3. Transport activity of wild type and mutants as measured by rhodamine123 efflux.

Molecular Pharmacology Fast Forward. Published on December 21, 2010 as DOI: 10.1124/mol.110.067611
This article has not been copyedited and formatted. The final version may differ from this version.

A: Rhodamine123 efflux is shown for the Q773R mutant as a representative example. An exponential curve was fitted to the data points taken at 1, 2, 3, 4 and 5 minutes according to the equation $y(MFU/cell) = a \times e^{-kt} + c$ where a is initial loading, e is Euler's number, k is the rate constant, t is the time in minutes and c is background fluorescence of the cells. The rate constant corresponds to the slope in the origin of the curve (-k*a, stippled black line) normalized to 1. Therefore, this rate constant is independent of initial loading (a), which is different for wild type and mutants and also between different experiments. The rate constant was measured in first order and thus represents a first order rate constant, which for each data point was determined in duplicate and plotted on the ordinate in Fig. 3B. **B**: First order rate constants were plotted as a function of P-gp surface expression, determined by MRK16 staining. For this figure a total number of 42 efflux experiments were performed in duplicate. In parallel, protein expression was determined. The slope of each linear regression line is a measure of relative transport activity (stippled lines). A linear least squares fit of wild-type P-gp (black) is shown by the stippled black line. Negative controls (blue triangles) lie close to that line with a y-offset corresponding to diffusion and an x-offset corresponding to background fluorescence of non-expressing cells. Mutants Q132A (yellow), Q773A (magenta) lie close to the stippled black line and therefore show transport rates that are comparable to wild-type. Q132R (green) and Q773R (orange) show transport rates of 52±13 and 24±6% of wild type, respectively (error propagation accounted for). The double mutant Q132R/Q773R (cyan) shows flux rates that are equal to simple diffusion (0.7-0.8/s).

Figure 4. Inhibition of rhodamine123 transport by propafenone analog GPV31 in wild type and mutant P-gp. Cells were loaded with rhodamine123 at 37°C for 30 minutes. Subsequently different concentrations of GPV31 were added to inhibit rhodamine123 efflux. **A**: For each concentration of

Molecular Pharmacology Fast Forward. Published on December 21, 2010 as DOI: 10.1124/mol.110.067611
This article has not been copyedited and formatted. The final version may differ from this version.

GPV31 (none: black, 0.008µM dark green, 0.02µM light blue, 0.05µM cyan, 0.13µM lavender, 0.32µM olive, 0.80µM dark blue, 2.00µM light green, 5.00µM red) a time dependent decrease in mean cellular fluorescence was monitored over four minutes. A representative experiment for Q773R P-gp is shown. An exponential curve was fitted by the method of least squares to data points taken at 60, 120, 180 and 240 seconds. First order rate constants were determined as described in the legend to Fig. 3A. These were then plotted as a function of GPV31 concentration as described (Ecker et al., 1999). Theoretically, the estimate for the zero time point (initial loading) should be identical for all curves. Values between 326 and 345 reflect experimental scatter. **B** shows the two concentration response curves for one representative experiment performed with the Q773R mutant. Filled squares correspond to the time dependencies shown in A, open squares are data points for the duplicate determination. The GPV31 concentration is shown on a logarithmic scale on the abscissa and first order rate constants of rhodamine123 transport are given on the ordinate. For this representative experiment IC_{50} values were determined to be 39 and 40nmol/l. Attention is drawn to the fact that the experimental protocol would not require normalization for protein expression, because IC_{50} values, in contrast to first order rate constants, are independent of protein expression.

C: Fractional inhibition of rhodamine123 transport is given as a percentage of first order rate constants in the absence of GPV31 for 6 independent experiments performed in duplicate. Note that IC_{50} values are independent of expression rates. The standard error of estimates for IC_{50} values is represented by horizontal error bars. Wild-type P-gp, black curve; Q132R, green curve; Q773R, orange curve. For IC_{50} values see Table 2.

Figure 5. Inhibition of rhodamine123 transport in wild-type and mutant P-gp by the non-protonable propafenone analog GPV366. The GPV366 concentration (0.08 to 50µM) is shown on a

Molecular Pharmacology Fast Forward. Published on December 21, 2010 as DOI: 10.1124/mol.110.067611
This article has not been copyedited and formatted. The final version may differ from this version.

logarithmic scale on the abscissa and fractional inhibition of rhodamine123 transport is on the ordinate. Fractional inhibition of rhodamine123 transport is given as a percentage of fluorescence in the absence of GPV366 to allow a composite graph of all experiments. Solid lines represent hyperbolic dose response curves, which were fitted to the data points by the method of least squares. IC_{50} values were calculated from these curves as 50% occupancy values and are represented as mean ± S.E (6 independent experiments; standard error of estimate represented as horizontal error bars). Wild type P-gp, black curve; Q132R, green curve; Q773R, orange curve. For details refer to the legend of Fig. 4.

Figure 6. Inhibition of rhodamine123 transport by verapamil in wild type and mutant P-gp. The composite graph shows fractional inhibition of rhodamine123 transport as a function of verapamil concentration of 5 independent experiments. Data points are given as mean ± S.E. of fractional inhibition values. IC_{50} values were calculated from concentration response curves as 50% occupancy values (standard error of estimate represented as horizontal error bars) as described in the legend to figure 4. Black curve: wild-type P-gp; green curve Q132R; orange curve Q773R. 1,080 individual data points were compiled for this graph. For IC_{50} values see Table 2. See legends for Figs. 4 and 5 for additional details.

Figure 7. Inhibition of rhodamine123 transport by vinblastine in wild type and mutant P-gp. The composite graph shows fractional inhibition of rhodamine123 transport as a function of vinblastine concentration of 3 independent experiments. Data points are given as mean ± S.E. of fractional inhibition values. IC_{50} values were calculated from concentration response curves as 50% occupancy values as described in the legend to figure 4. Black curve: wild-type P-gp; green curve Q132R; orange curve Q773R. For IC_{50} values see Table 2.

Molecular Pharmacology Fast Forward. Published on December 21, 2010 as DOI: 10.1124/mol.110.067611
This article has not been copyedited and formatted. The final version may differ from this version.

Table 1. Quality of models as assessed by Modeller (Melo and Sali, 2007; Shen et al., 1995; Shen and Sali, 2006), ProQ (Wallner and Elofsson, 2003) and Procheck (Laskowski et al., 1993). The MODELLER DOPE-score is a statistical potential energy-score trained to recognize correct folding by analyzing nonbonding interactions between atoms in a pair-wise fashion. The more negative the number, the higher the likeliness, that a correctly folded model was obtained. The GA341 score is a statistical potential for correct local model geometry. Four parameters contribute to this score: backbone phi and psi angles, atom overlap, atom probability density function and exposed surface area. The score ranges between 0 and 1, where 1 is indicative of a correctly folded model. A ProQ LG score above 1.5 is indicative of a correct, above 3 of a good and above 5 of a very good model. A MaxSub score > 0.1 indicates a correct model, a score of > 0.5 shows a good and > 0.8 a very good model, whereby the LG score performs better with larger proteins such as P-gp and the MaxSub score is optimized for shorter proteins. ProCheck classifies dihedral angles in favorable, allowed, generously allowed and disallowed regions of a Ramachandran plot.

Molecular Pharmacology Fast Forward. Published on December 21, 2010 as DOI: 10.1124/mol.110.067611
This article has not been copyedited and formatted. The final version may differ from this version.

	Sav 1866 based model	Data-driven model	MDR1A based model
Modeller			
DOPE	-140414	-149326	-130736
GA341 score	1.0	1.0	1.0
ProQ			
ProQ LGscore	4.78	5.62	3.82
ProQ MaxSub	0.30	0.31	0.25
ProCheck			
most favorable	94.3%	94.3%	86.2%
additionally allowed	5.2%	5.3%	10.3%
generously allowed	0.4%	0.2%	2.2%
disallowed	0.1%	0.2%	1.3%

Molecular Pharmacology Fast Forward. Published on December 21, 2010 as DOI: 10.1124/mol.110.067611
This article has not been copyedited and formatted. The final version may differ from this version.

Table 2. IC_{50} values for rhodamine123 efflux inhibition by verapamil, vinblastine and propafenone analogs.

IC_{50} values were calculated from concentration response curves (shown in Figs 4, 5, 6 & 7). Results are represented as mean ± standard deviation of at least three individual experiments performed in duplicate. A significant difference from wild type values is indicated by an asterisk (*$p < 0.05$).

Mutation	**IC_{50} (µM) ± SD**			
	Verapamil	**Vinblastine**	**GPV31**	**GPV366**
Wild type P-gp	0.43 ± 0.10	2.68 ± 0.93	0.11 ± 0.06	2.60 ± 0.69
Q132A	0.30 ± 0.07	2.58 ± 0.31	0.10 ± 0.03	2.57 ± 0.69
Q773A	0.42 ± 0.15	2.80 ± 0.12	0.11 ± 0.05	2.40 ± 1.47
Q132A/Q773A	0.44 ± 0.16	2.24 ± 0.43	0.12 ± 0.01	2.87 ± 0.63
Q132R	1.24 ± 0.13*	9.19 ± 1.20	0.71 ± 0.46*	2.64 ± 0.59
Q773R	0.14 ± 0.04*	0.45 ± 0.16	0.02 ± 0.01*	2.09 ± 0.90

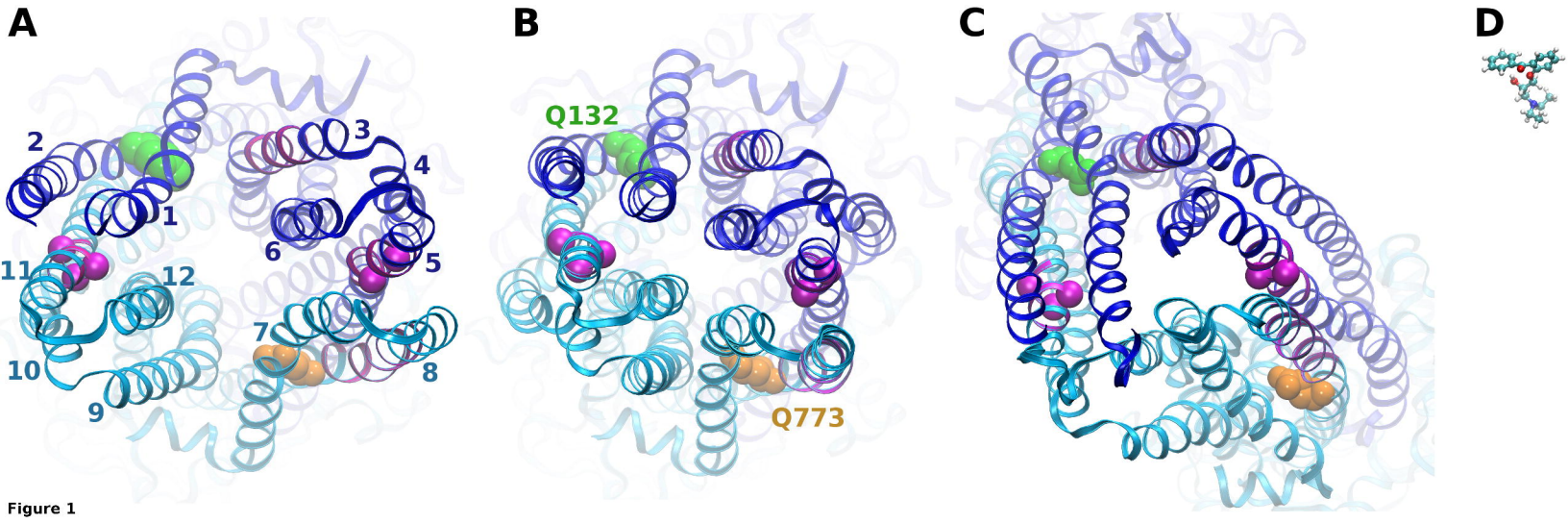

Figure 1

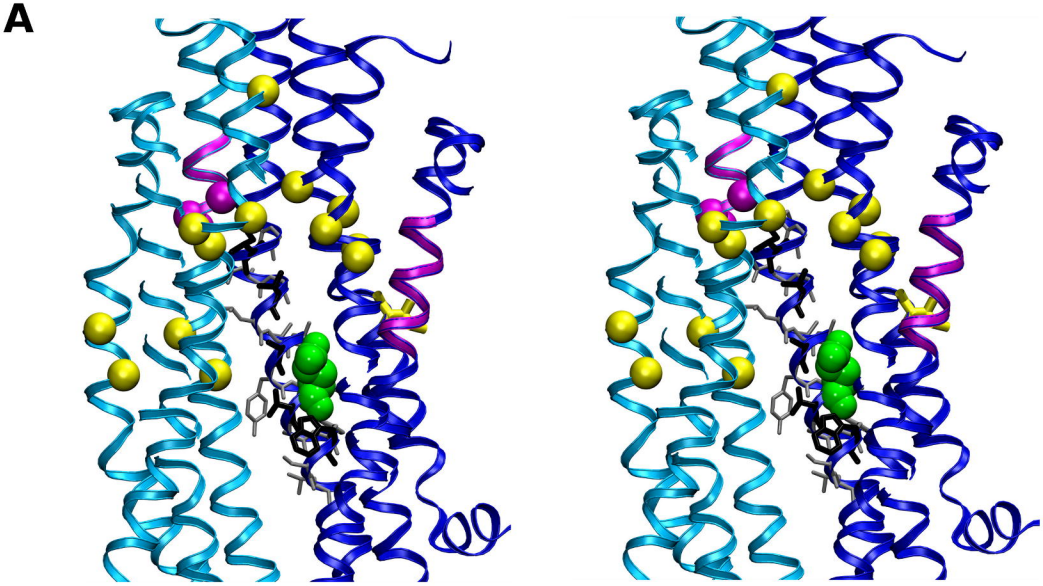

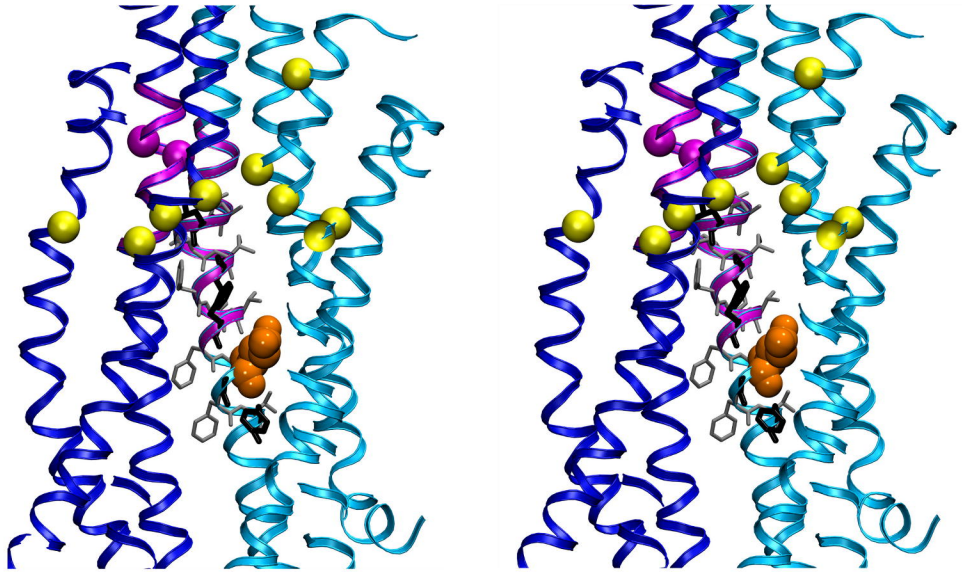

C

Cons. score	H2	Main exposure	H8	Cons. score
62	S	Lipid	L	94
90	G	Lipid	A	42
92	I	**Pore**	L	83
90	G	Helix	G	90
63	A	Lipid	I	67
73	G	Lipid	I	85
90	V	**Pore**	S	85
96	L	Helix	F	90
61	V	Lipid	I	66
29	A	Helix	T	97
88	A	**Pore**	F	70
84	Y	Helix	F	89
100	I	Lipid	L	58
100	Q	**Pore**	Q	100
89	V	**Pore**	G	100
78	S	Lipid	F	90
47	F	Lipid	T	72
88	W	**Pore**	F	93

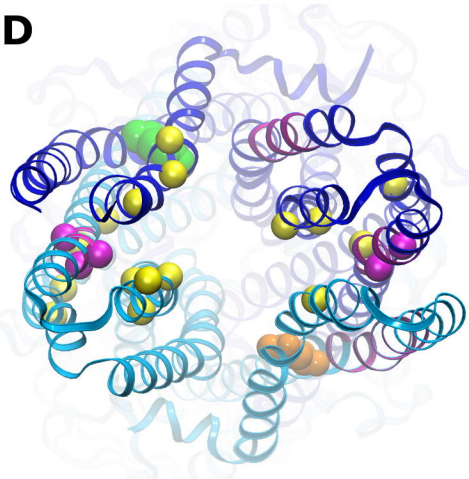

Figure 2

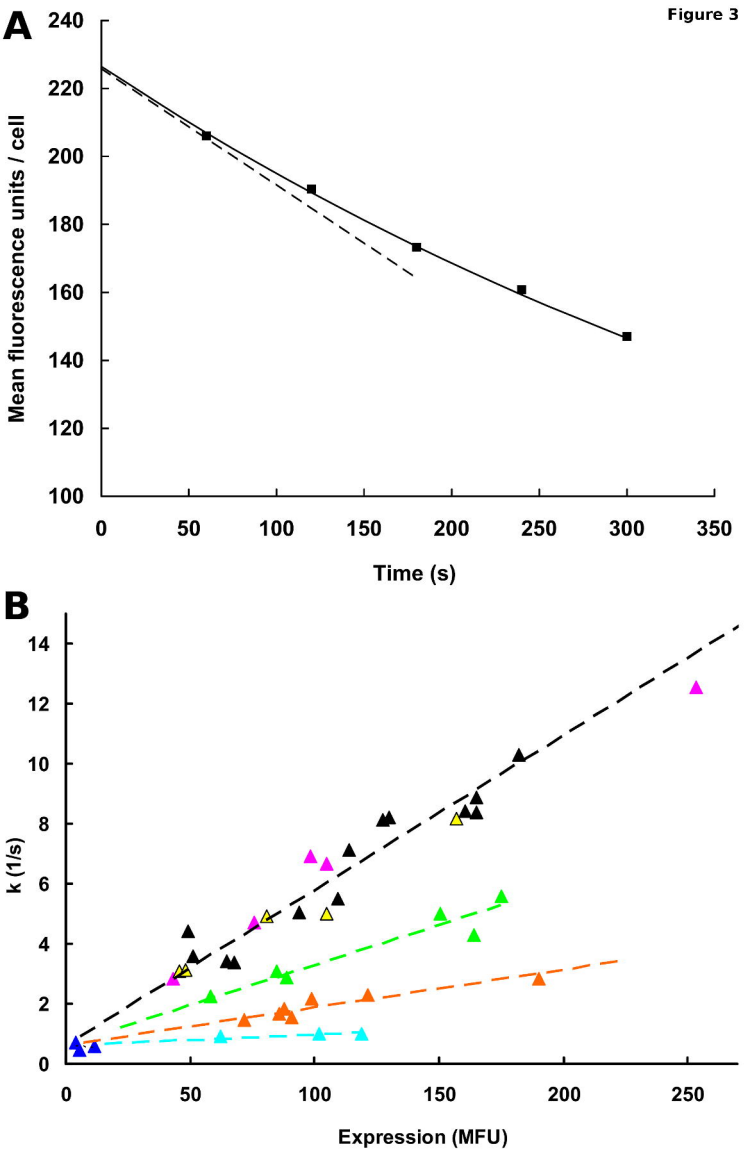
A
240
220
200
180
160
140
120
100
Mean fluorescence units / cell
0
50
100
150
200
250
300
350
Time (s)
B
14
12
10
8
6
4
2
0
k (1/s)
0
50
100
150
200
250
Expression (MFU)

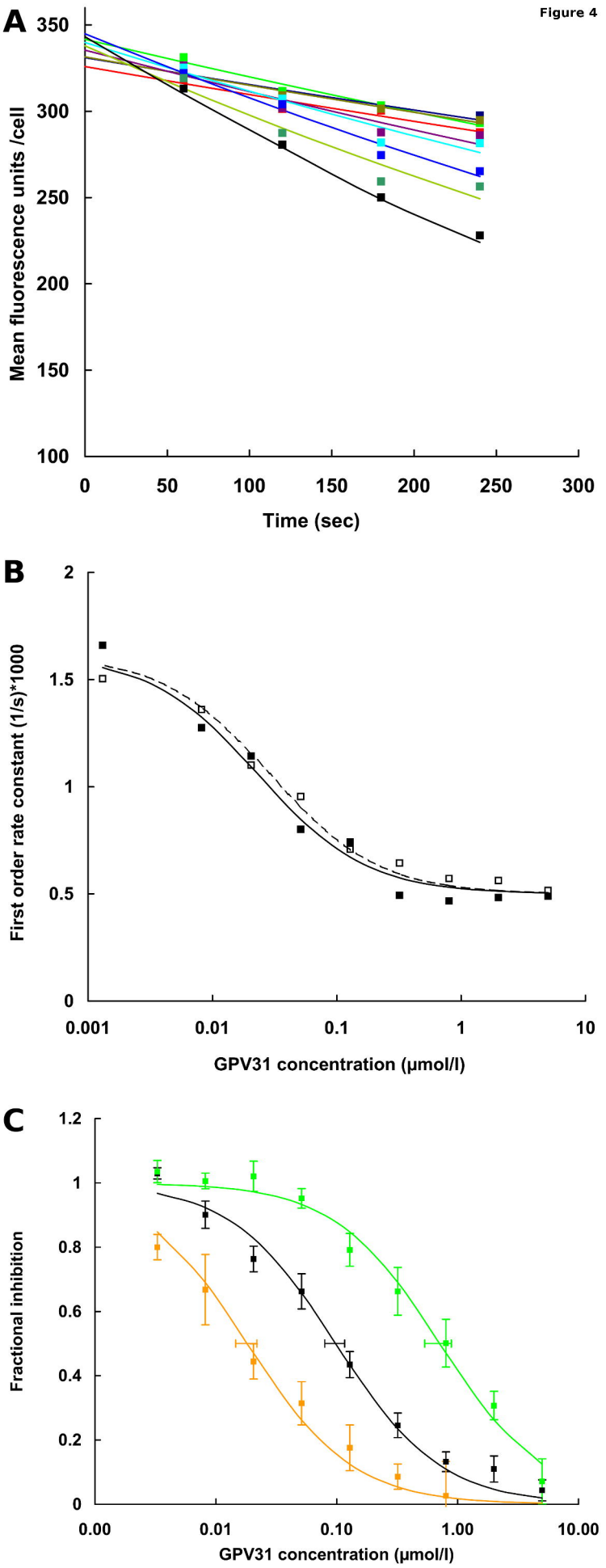
A
Mean fluorescence units /cell
350
300
250
200
150
100
0
50
100
150
200
250
300
Time (sec)
B
First order rate constant (1/s)*1000
2
1.5
1
0.5
0
0.001
0.01
0.1
1
10
GPV31 concentration (µmol/l)
C
Fractional inhibition
1.2
1
0.8
0.6
0.4
0.2
0
0.00
0.01
0.10
1.00
10.00
GPV31 concentration (µmol/l)

Figure 5

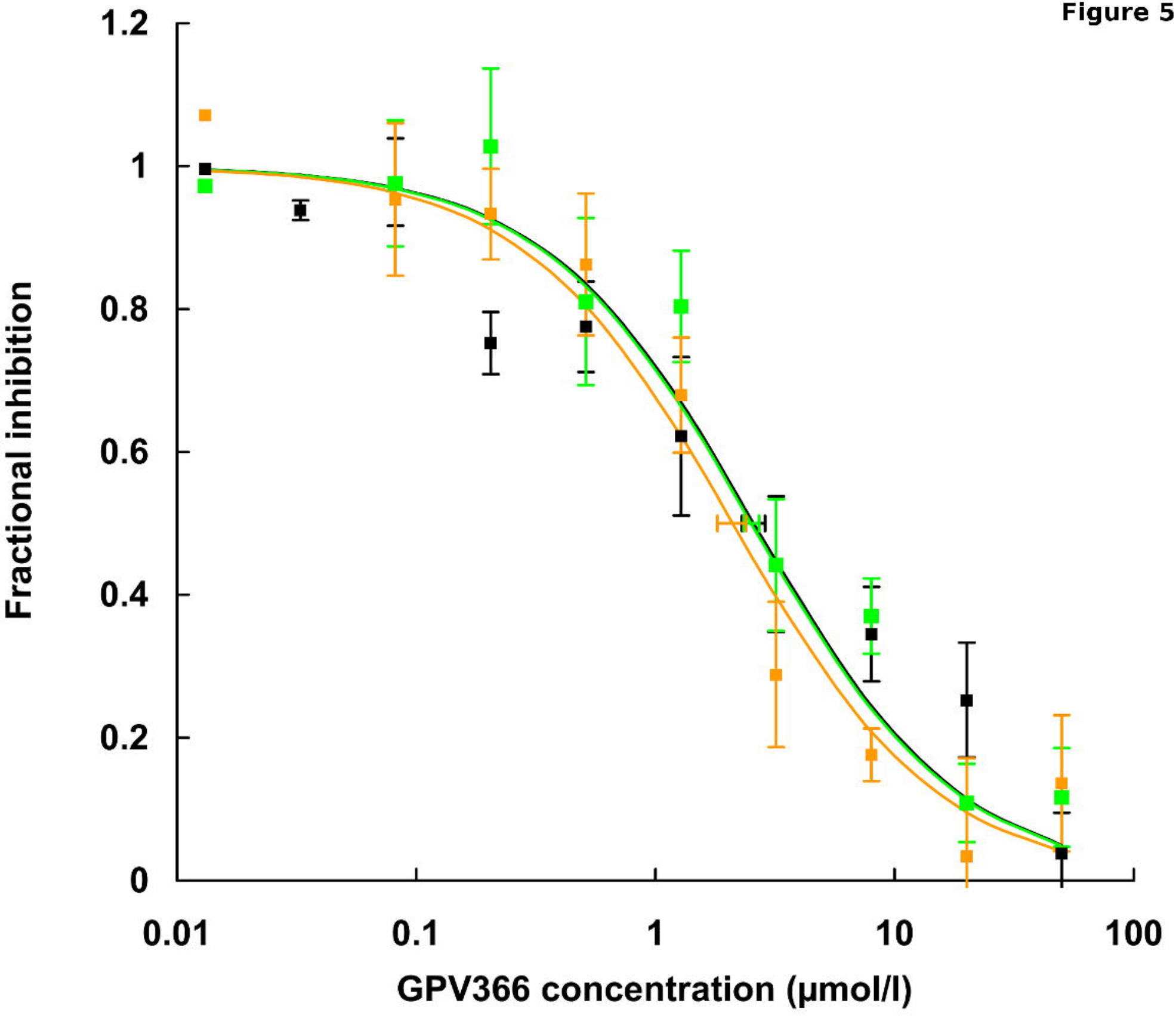
1.2
1
0.8
0.6
0.4
0.2
0
Fractional inhibition
0.01
0.1
1
10
100
GPV366 concentration (µmol/l)

Figure 6

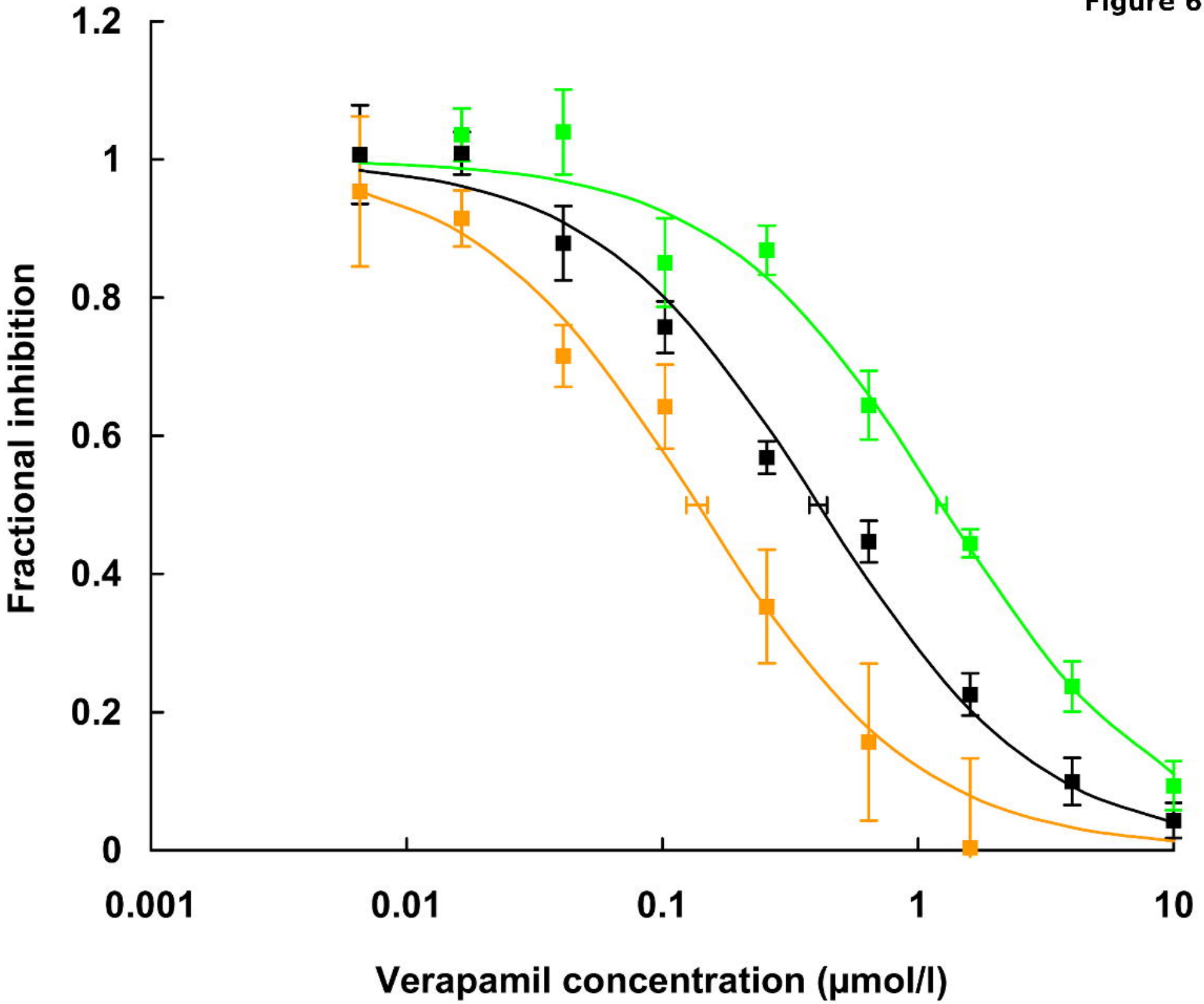
1.2
1
0.8
0.6
0.4
0.2
0
Fractional inhibition
0.001
0.01
0.1
1
10
Verapamil concentration (µmol/l)

Figure 7

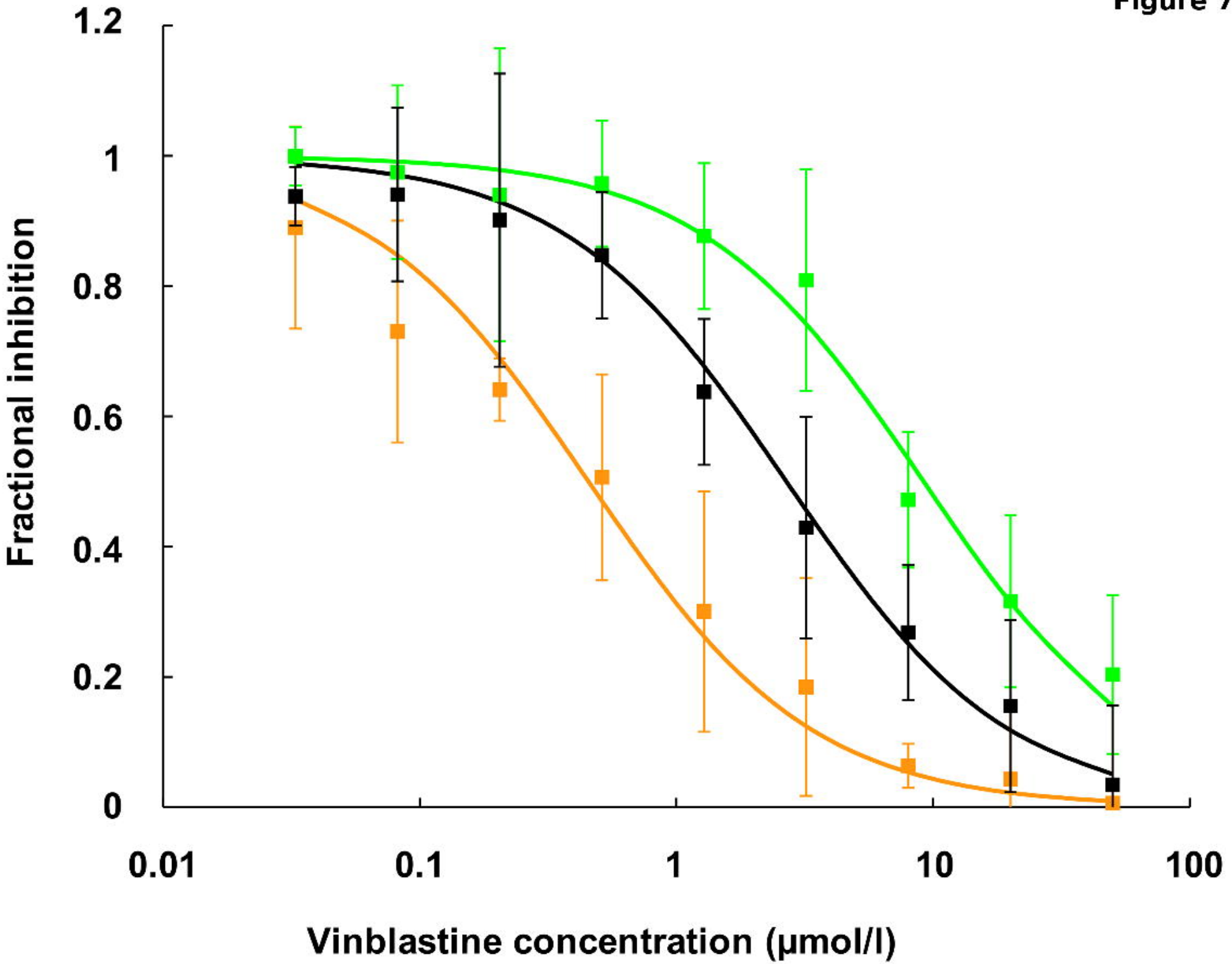
1.2
1
0.8
0.6
0.4
0.2
0
Fractional inhibition
0.01
0.1
1
10
100
Vinblastine concentration (µmol/l)